MOBSTER - VII. Using light curves to infer magnetic and rotational properties of stars with centrifugal magnetospheres

I. D. Berry,[1]★ M. E. Shultz,[1] S. P. Owocki,[1,2] A. ud-Doula[3]

[1]*Department of Physics & Astronomy, University of Delaware, Newark, DE 19716, USA*
[2]*Bartol Research Institute, University of Delaware, Newark, DE 19716, USA*
[3]*Penn State Scranton, 120 Ridge View Dr., Dunmore, PA 18512, USA*

ABSTRACT

Early-type B stars with strong magnetic fields and rapid rotation form centrifugal magnetospheres (CMs), as the relatively weak stellar wind becomes magnetically confined and centrifugally supported above the Kepler co-rotation radius. Using a purely dipolar magnetic field topology, CM plasma is concentrated at and above the Kepler co-rotation radius at the intersection between the rotation and magnetic field axis. Stellar rotation can bring these clouds of material in front of the star, leading to photometric eclipses. However, for stars with strong (~ 10 kG) magnetic fields and rapid rotation, CMs can become optically thick enough for emission to occur via electron scattering. Using high-precision space photometry from a sample of stars with strong Hα emission, we apply simulated light curves from the Rigidly Rotating Magnetosphere model to directly infer magnetic and rotational properties of these stars. By comparing the values inferred from photometric modelling to those independently determined by spectropolarimetry, we find that magnetic obliquity angle β, viewer inclination i and critical rotation fraction W can be reliably recovered. However, there are large discrepancies between the optical depth at the Kepler radius $\tau_{\rm K}$ expected from magnetometry, and the values required to match the observations. We show that $\tau_{\rm K}$ of order unity is needed to reasonably match the light curve morphology of our sample stars.

Key words: stars: early-type – stars: massive – stars: circumstellar matter – stars: magnetic field – stars: individual (HD 37479, HD 142184, HD 182180, HD 345439)

1 INTRODUCTION

Hot, luminous and massive O and B stars have dense line-driven stellar winds (Castor et al. 1975; Gayley 1995; Vink et al. 2001). A small but significant subset ($\sim 10\%$) host magnetic fields (Grunhut et al. 2017; Sikora et al. 2019b) with strengths on the order of 100s of G to 10s of kG (Sikora et al. 2019c; Petit et al. 2019; Sikora et al. 2019b; Shultz et al. 2019b). The vast majority of these magnetic fields show simple topologies, with most being well approximated by dipoles tilted with respect to the rotational axis (Kochukhov et al. 2019). The combination of a dense ionized stellar wind and a strong magnetic field allows plasma to become magnetically trapped by magnetic field loops, forming a circumstellar magnetosphere (Bolton et al. 1987; Babel & Montmerle 1997; ud-Doula & Owocki 2002), which is forced into co-rotation with the magnetic field.

The structure of such circumstellar magnetospheres depends strongly on the stellar rotation. Magnetic O stars tend to be slow rotators due to magnetic torque applied onto their very strong winds leading to rapid loss of angular momentum (ud-Doula et al. 2009; Petit et al. 2013). Slow rotation means that the Kepler co-rotation radius ($R_{\rm K}$) is well beyond the Alfvén radius ($R_{\rm A}$), the maximum distance of closed magnetic field loops. As such, trapped stellar wind material lacks centrifugal support to counteract gravity, and so falls back down to the stellar surface on dynamical timescales. This is known as a "dynamical magnetosphere" (DM; ud-Doula & Owocki 2002; Petit et al. 2013).

Spectral type B stars are less luminous than O stars. A consequence of this is that their line driven winds aren't nearly as powerful and dense as O stars. The magnetic torque applied to the winds of B stars is then much less than that of O stars, leading to shorter periods of rapid rotation (N.B. there is one O star with a CM, Plaskett's Star; Grunhut et al. 2012b; Grunhut et al. 2022. There are also several B stars without CMs, e.g. the ultra-slow rotator ξ^1 CMa; Shultz et al. 2017, 2018b; Erba et al. 2021). In general, B stars exhibit such rapid rotation that the Kepler co-rotation radius usually falls below the Alfvén Radius. In this scenario, material fed into the magnetosphere at or above $R_{\rm K}$ now has the centrifugal support to remain suspended above the surface, but is stopped from flowing further by closed magnetic field loops. This trapped plasma accumulates into dense clouds in the region between $R_{\rm K}$ and $R_{\rm A}$ forming a structure called a "centrifugal magnetosphere" (CM; Townsend & Owocki 2005; ud-Doula et al. 2008; Petit et al. 2013). Many B-type stars have $R_{\rm K}$ within half a stellar radius of the photosphere, rendering their magnetospheres almost entirely centrifugal

For B stars, the relative strengths of the magnetic field and the stellar wind outflow can be large enough such that the magnetic field is completely dominant over stellar wind material out to tens of stellar radii. This justifies the "rigidly rotating magnetosphere"

★ email: ianbass@udel.edu

(RRM) model developed by Townsend & Owocki (2005) which finds the accumulation surface of a CM with a tilted dipole under the key assumption that the magnetic field remains completely rigid and unperturbed by the presence of circumstellar material out to large radii.

While RRM assumes a completely rigid magnetic field, regardless of the amount of material within the magnetosphere, in reality all magnetic fields have a finite strength, and hence a finite rigidity. This means at some point, centrifugal force acting on the accumulating plasma will overpower magnetic tension. This is known as centrifugal breakout (CBO), first suggested to be the mechanism by which plasma is ejected from stellar magnetospheres by Havnes & Goertz (1984), who examined and rejected ambipolar diffusion as a plausible alternative. Further analysis is given in the Appendix of Townsend & Owocki (2005), which provided scalings for density, timescale and breakout-limited asymptotic mass.

Townsend et al. (2013) challenged large-scale magnetosphere emptying via CBO events using the *MOST* (Microvariability and Oscillations in Stars; Walker et al. 2003) satellite to measure photometric variability of σ Ori E over three weeks. These observations found no evidence of large-scale magnetospheric emptying and reorganization as suggested by Magnetohydrodynamic (MHD) simulations presented by ud-Doula et al. (2006) and ud-Doula et al. (2008). This led to the development of a new model by Owocki & Cranmer (2018), in which CM plasma transport is governed via a gradual "leakage" by diffusion across magnetic field loops. However, analysis by Owocki et al. (2020) and Shultz et al. (2020) showed that the onset, emission strength, and line profile morphologies of Hα emission in CMs of B-type stars can only be explained by constant CBO events.

Magnetic B-stars often exhibit radio emission from gyrosynchrotron and electron cyclotron maser emission. Recent radio observations by Das & Chandra (2021) report the first observation of a "giant pulse" from the star CU Vir, larger than any seen previously, which they speculated could be linked to a large-scale CBO event since the enhanced emission came from both magnetic hemispheres. Leto et al. (2021) conclusively demonstrated that the previous wind-powered current sheet model for electron acceleration (e.g. Trigilio et al. 2004) was inconsistent with the radio luminosities and mass-loss rates of magnetic stars, and found a rotationally-dependent luminosity scaling for gyrosynchrotron emission, suggesting CBO as a possible mechanism driving electron acceleration. This relationship was confirmed by the larger sample analyzed by Shultz et al. (2022), who also found a close relation between Hα emission strength and radio luminosity, further supporting CBO as a common mechanism. Owocki et al. (2022) then demonstrated that the gyrosynchrotron scaling relationship can be explained as a consequence of magnetic reconnection during CBO events, which accelerates electrons to the required semi-relativistic energies.

In their original analysis of CBO, Townsend & Owocki (2005) assumed that the magnetosphere was last emptied out at some arbitrary time in the past, with the density at some later time set by the wind feeding rate, which is proportional to the magnetic field strength. However, as demonstrated by Townsend et al. (2013), there is no evidence of the large-scale, magnetosphere-emptying breakout events in photometric time series, a conclusion supported by Shultz et al. (2020), who found Hα profiles to be unchanged across more than 20 years. Since magnetospheric diagnostics are consistent with the visible material being always just at the breakout density, Shultz et al. (2020) and Owocki et al. (2020) speculated that CBO must be continuously occuring on small spatial scales. Calibrating their analysis with the MHD simulations performed by ud-Doula et al. (2006, 2008), Owocki et al. (2020) found that CBO implies a radial surface density that varies with the square of the magnetic field strength. This leads to a steeper radial decline in density, but an overall higher density within the CM (Owocki et al. 2020). This higher density means that electron scattering can lead to a significant and detectable amount of magnetospheric emission (Berry et al. 2022).

Photometric variation can be dominated by the presence of a CM, with the prototypical example of this found from the B2Vp star σ Orionis E (HD 37479, henceforth σ Ori E; Landstreet & Borra 1978). This star shows photometric variability due to a cloud forced into co-rotation by σ Ori E's ~10 kG (Oksala et al. 2012) magnetic field. Two major dips in brightness are visible during this star's 1.19 day rotation period, with photometric minima occurring simultaneously with phases of magnetic nulls (i.e. phases corresponding to views perpendicular to the magnetic field axis). Landstreet & Borra (1978) were the first to suggest that such variation is due to co-rotating, magnetically trapped plasma, with photometric minima occurring when material eclipses the star. This idea received strong support when Townsend et al. (2005) fit the light curve of σ Ori E obtained by Hesser et al. (1977) with the RRM model. Further analysis of the light curve of σ Ori E was done by Oksala et al. (2015), who employed an arbitrary rigidly rotating magnetosphere (aRRM) model based on a Zeeman-Doppler imaging map to simulate a light curve with contributions from surface spots. Oksala et al. (2015) found that this model could match eclipse depth and width with a viewer inclination of 85°, but could not match out-of-eclipse variability even after including chemical spot contributions inferred from Doppler Imaging maps.

Models of CMs have been used to explore photometric variation for a range of magnetic tilt angles, observer inclinations and rotation periods. Townsend (2008) demonstrated that prominent circumstellar eclipses can only be detected with highly tilted magnetic fields at high viewer inclination with respect to the rotational axis. Photometric variation from O stars via eclipsing DMs was explored by Munoz et al. (2020), who used the Analytical Dynamical Magnetosphere model developed by Owocki et al. (2016).

Circumstellar eclipsing is not the only mechanism in which rotationally modulated variation can occur with magnetic stars. These stars are almost invariably chemically peculiar (CP; e.g. Kochukhov & Bagnulo 2006; Sikora et al. 2019a), with σ Ori E, a helium-rich star, falling into this category. Chemical peculiarities in such stars are not homogeneous across the surface, and often are clumped together in abundance patches. These chemical abundance spots lead to periodic variation as the star rotates (e.g. Renson & Catalano 2001; Krtička et al. 2007, 2009; Krtička et al. 2013; Sikora et al. 2019c).

Berry et al. (2022) conducted a similar study to Townsend (2008), covering a parameter space consisting of magnetic tilt angle β, viewer inclination with respect to the rotation axis i, critical rotation fraction W and optical depth at the Kepler co-rotation radius $\tau_{\rm K}$. However, Berry et al. (2022) also took emission from CMs via electron scattering into account, where Townsend (2008) had only considered absorption. Berry et al. (2022) used a Centrifugal-Breakout (CBO) modified (Owocki et al. 2020) and MHD calibrated (ud-Doula 2021) form of the RRM model, and found similar results to Townsend (2008), with the addition that CMs can become sufficiently optically thick (i.e. $\tau_{\rm K} \geq 1$) in the continuum to give up to 5% extra emission above the stellar flux due to circumstellar scattering.

Recent work done by Krtička et al. (2022) investigated the magnetospheric structure and light curve morphology for magnetospheres governed by higher-order magnetic multipoles. Both magnetospheric absorption and emission from electron scattering were considered, similar to the models presented by Berry et al. (2022). However,

Krtička et al. (2022) made approximations when they solved the radiative transfer equation, whereas Berry et al. (2022) made no simplifications and fully solved radiative transfer assuming a scattering source function. Overall Krtička et al. (2022) found that tiny features seen in light curve morphologies not accounted for by models with simple dipoles can be matched by RRM models generated using magnetic fields dominated by higher order multipoles.

The work presented here uses photometry from a number of high-precision space photometers, one of which is the Transiting Exoplanet Survey Satellite (*TESS*). These data are fit with our RRM-CBO models, which allow us to infer rotational properties solely from photometric time-series. This is a primary goal of the MOBSTER collaboration (Magnetic OB(A) Stars with *TESS*: probing their Evolutionary and Rotational properties; David-Uraz et al. 2019), where *TESS* is used to increase the number of known rotational periods for magnetic chemically peculiar stars, which can then be utilized to infer evolutionary and magnetospheric properties of these stars.

Previous light curve models of CMs have been performed using forward modeling, with the light curve derived from a known magnetic field geometry (e.g. Townsend et al. 2005; Oksala et al. 2015; Krtička et al. 2022). In this paper, we perform a blind test of the models, using light curves of four stars to derive geometrical, rotational and opacity parameters without reference to the values determined from spectroscopy, magnetometry and evolutionary models. These are then compared to the parameters presented by Shultz et al. (2019b). The targets – σ Ori E, HD 142184, HD 182180, and HD 345439 – were selected on the basis that they have well-constrained magnetic, stellar, and rotational properties, and have available space photometry with light curves that, at least by eye, appear to be magnetospherically dominated. All four have extremely strong Hα emission, amongst the strongest of the large sample of Hα-bright CM stars examined by Shultz et al. (2020). This extremely strong Hα emission, and the finding by Oksala et al. (2015) that the contribution of chemical spots to σ Ori E's light curve is negligible as compared to the magnetospheric contribution, underlie our assumption that the light curves of these stars can be reproduced with purely magnetospheric models.

Observations are described in Section 2. Techniques for our model fitting are given in Section 3. Results for individual stars are provided in Section 4. Implications of this work are discussed in Section 5. Finally, summaries and conclusions are given in Section 6.

2 OBSERVATIONS

Photometry for the HD 182180 *K2* light curve was obtained from the Mikulski Archive for Space Telescopes (MAST). The NASA *Kepler* satellite is a μmag-precision space photometer originally intended for long duration observations to detect exo-planets via the transit method. The photometer has a 110 square degree field of view and operates in the 400 – 850 nm bandpass. The *K2* (Howell et al. 2014) mission began following the failure of *Kepler's* reaction wheels. Incoming solar wind allowed *Kepler* to be stabilized and observe fields along the ecliptic for roughly 3 months at a time. HD 182180 was observed by *Kepler* during campaign 7 with observations lasting from 2015 October 04 to 2015 December 26. HD 182180 was observed in long-cadence mode with exposures lasting 30 minutes each.

σ Ori E and HD 345439 were observed by the Transiting Exoplanet Survey Satellite (*TESS*) (Ricker et al. 2015). *TESS* is a space photometer intended to search for transiting exo-planets, using four cameras with a $24^\circ \times 96^\circ$ field of view covering 600 – 1050 nm wavelengths. *TESS's* two year mission began in 2018 in which 13 sectors were covered each year, observed for 27 days each.

σ Ori E was observed by TESS in sector 6 from 2018 December 15 to 2020 December 16 with a two-minute cadence. σ Ori E *TESS* data were acquired via MAST.

HD 345439 was observed by *TESS* in sector 41 from 2021 July 24 to 2021 August 20 during *TESS's* extended mission. *TESS's* two minute cadence was used. *TESS* photometric data were obtained via MAST.

Photometric data for HD 142184 is the same taken by the Microvariability and Oscillations of STars (*MOST*; Walker et al. 2003) satellite presented by Grunhut et al. (2012a). The Canadian Space Agency *MOST* satellite was a space photometer dedicated to asteroseismology, in which photometry was obtained using a visible-light dual-CCD camera and a 15-cm aperture Maksutov telescope. Photometric measurements of HD 142184 were done by aperture photometry on a 20×20 pixel subgrid on the MOST CCD photometer. Observations were done in switched-target mode, with part of the orbital phase being shared with observations of Arcturus. Each observation of HD 142184 contained 157 stacked 0.18 second exposures.

The Python package *Lightkurve* (Lightkurve Collaboration et al. 2018) was used to process the photometric data of each star, with outlier rejection, binning, and normalization done on each light curve using *Lightkurve's* built-in algorithms. The rotational periods for σ Ori E ($1.1908228^{+0.0000012}_{-0.0000010}$ d; Townsend et al. 2010), HD 142184 ($0.508276^{+0.000015}_{-0.000012}$ d; Grunhut et al. 2012a), HD 182180 (0.521428 ± 0.000006 d; Rivinius et al. 2008) and HD 345439 (0.7701 ± 0.0003 d; Wisniewski et al. 2015) were adopted from previous literature.

3 MODEL FITTING TECHNIQUES

Let us now discuss fitting models from Berry et al. (2022) to the light curves of the stars discussed in Section 2. The model light curves themselves are grounded in the same physics as presented by Berry et al. (2022). Photometric modulation in these models is due to both absorption and electron scattering emission as a result of a co-rotating CM. The magnetic field in these models is a centered tilted dipole, with contributions from higher order magnetic multipoles neglected. The light curves can be modified by changing four main parameters: magnetic obliquity β, viewer inclination from the rotation axis i, optical depth at the Kepler radius τ_K, and critical rotation fraction $W \equiv V_{rot}/V_{orb}$ where V_{rot} is the star's equatorial rotational velocity and V_{orb} is the star's surface orbital velocity.

Other parameters were used to control the structure of the magnetosphere, including a "latitudinal scale length" χ (discussed further by Berry et al. 2022), which controls the azimuthal distribution of density in the CM in accordance with recent MHD simulations presented by ud-Doula (2021). The ratio between thermal energy and gravitational escape energy at R_K, denoted ϵ, is also utilized. This effectively controls the disk thickness and scale height $h_m \approx \sqrt{2\epsilon/3}$ (see Berry et al. 2022, for further details). For all models shown in the present work, we fixed $\chi = 0.05$ and $\epsilon = 0.01$, with the latter giving an associated scale height $h_m = 0.082\, R_K$.

The light curve models presented by Berry et al. (2022) spanned the ranges of $30^\circ \leq \beta \leq 75^\circ$, $30^\circ \leq i \leq 90^\circ$, $0.5 \leq \tau_K \leq 2$ and $0.25 \leq W \leq 0.75$. When doing the model fitting with the four aforementioned stars, it was deemed necessary to expand the grid of these parameters, as certain stars had best fit models that were on the edge of the parameter grid. As such, we expanded the grid to $10^\circ \leq \beta \leq 88^\circ$, $0.1 \leq \tau_K \leq 4$, $0.1 \leq W \leq 0.75$. New values of viewer inclination i smaller than 30° were deemed unnecessary to

add, as the viewer inclination for these stars is expected to be large given the amount of variability.

In order to perform a precise fitting of the light curves, the grid needed to be sampled with small step sizes. However, calculating models from first principles is rather slow and expensive due to having to solve the radiative transfer equation for electron scattering (see Berry et al. 2022). Therefore we implemented an interpolation algorithm which allowed us to quickly generate a model of any combination of the four parameters that falls within the parameter grid. To do this we used the spline interpolation from the *Series* functions from the *Pandas* Python package.

To perform the fitting with our models and the observations, the light curves for each star are first normalized by *Lightkurve* to the median flux value. However, the RRM-CBO models we use for the fitting are normalized to the base flux of the star if there were no magnetosphere present. Since there is no guarantee that the median flux of the measured light curve reflects the unobstructed light of the star, it was necessary to shift the empirical light curves vertically in flux to ensure the best fit possible with each model. Given that a number of these stars exhibit a primary and secondary eclipse, the data is shifted such that the minimum values of both the data and the models are equal, so that the primary eclipse is prioritized to be fit over any secondary eclipses. Furthermore, we opted to have phase 0 coincide with the absolute minimum in the star's light curves. In our models phase 0 is set to occur when the magnetic field axis is pointing towards the observer, which does not coincide with a photometric minimum. Because of this, the models are shifted in phase to ensure the best fit between the models and the data. After these shifts are performed, we use reduced χ^2 in order to determine goodness-of-fit between our models and observations.

Following our model fitting, we compare our best fit parameter values to those reported by Shultz et al. (2019b), which involves calculating the associated τ_K for electron scattering. The appendices of Townsend & Owocki (2005) provide a CBO scaling for the peak surface density of the CM at R_K:

$$\sigma_K = c_f \frac{B_K^2}{4\pi g_K}, \tag{1}$$

where $B_K = B_{eq}/R_K^3$ and $g_K = GM_*/R_K^2$ are respectively the equatorial magnetic field strength and gravitational acceleration at R_K. c_f is a correction factor found via comparison with MHD simulations of magnetospheres, by which Owocki et al. (2020) found $c_f \approx 0.3$. Furthermore, Berry et al. (2022) introduced a surface density scaling for the magnetosphere:

$$\sigma(r, \theta_o) = \sigma_K \left(\frac{r}{R_K}\right)^{-p} \exp\left(-\cos^2\theta_o/\chi\right) \tag{2}$$

where θ_o is the co-latitude, σ_K is defined by Equation 1, and χ is the latitudinal scale length introduced above. p is the radial drop-off index, where $p = 5$ in the models presented by Berry et al. (2022) and used here. This, along with the canonical electron scattering opacity $\kappa_e = 0.344\,\mathrm{cm}^2/\mathrm{g}$, and the fact that the polar magnetic field strength is twice that of the equatorial field strength (i.e. $B_* = 2B_{eq,*}$), we arrive at an expression for τ_K:

$$\tau_K = \kappa_e \sigma_K = c_f \kappa_e \frac{B_*^2}{16\pi g_*} \left(\frac{R_K}{R_*}\right)^{-4} = c_f \kappa_e \frac{B_*^2}{16\pi g_*} W^{8/3}, \tag{3}$$

where $g_* = GM_*/R_*^2$ is the surface gravitational acceleration. The right hand side of Equation 3 uses the relation (ud-Doula et al. 2008):

$$R_K = W^{-2/3} R_*. \tag{4}$$

Equation 3 shows that τ_K is a function of M_*, R_*, W, and B_*, each of which we can find in the tables of Appendix C by Shultz et al. (2019b) and shown again here in Table 1. For a correction factor $c_f = 0.3$, Equation 3 shows that CMs around rapidly rotating magnetic B stars should typically be marginally optically thick (i.e. τ_K is of order unity) in the continuum. Furthermore, we see that τ_K is dependent on the square of the surface polar magnetic field strength, which in the case of a simple dipole declines as $B_* \sim r^{-3}$. Thus the optical depth in the continuum falls off rapidly with distance (i.e. $\tau_K \sim B_*^2 \sim r^{-6}$) and so most magnetospheric emission remains close to R_K.

4 LIGHT CURVE FITTING

In this section we present our best fit light curves for σ Ori E, HD 142184, HD 182180 and HD 345439, as well as reduced χ^2 contour plots to visualize degeneracies in parameter space and the associated fit uncertainties. Along with our best-fit models, we show for comparison forward modeled light curves calculated using the parameters presented by Shultz et al. (2019b), and provided here in Table 1. Note that τ_K is a free parameter in the forward modeled light curves, rather than τ_K found from Equation 3 which gives τ_K values that are either too small or large for a reasonable fit.

4.1 σ Ori E

σ Ori E is a rapidly rotating magnetic B2Vp helium-rich star and the prototypical example of a star whose photometric variation is mainly due to the presence of a rigidly rotating circumstellar magnetosphere (Townsend et al. 2005). This star hosts a relatively strong (~ 10 kG) oblique ($47° \leq \beta \leq 59°$; Oksala et al. 2015) magnetic field and a relatively fast ($W \approx 0.2$; Shultz et al. 2019b) rotation speed. Viewer inclination is expected to be high given the large range of variation seen with σ Ori E, indeed quite close to 90° (Oksala et al. 2015). With this, the continuum optical depth of the CM around σ Ori E should be large enough for electron scattering to provide a small but significant amount of emission in its light curve. Indeed, the light curve of σ Ori E shows what may be a small emission bump at phase 0.6 (see Hesser et al. 1977; Landstreet & Borra 1978; Townsend et al. 2005), recently reproduced by Krtička et al. (2022), and the main point of motivation for the work done by Berry et al. (2022).

Other sources of photometric variation are present for σ Ori E, one of which is surface abundance spots. However, surface abundance spots alone are not enough to reproduce the out-of-eclipse variability displayed by σ Ori E (Oksala et al. 2015). This shows that a co-rotating magnetosphere must be the dominant source of photometric variation.

σ Ori E *TESS* data is contaminated by light from the nearby O star σ Ori AB. To account for this, it is necessary to scale the data. From light curves shown in previous work (Landstreet & Borra 1978; Townsend et al. 2010; Oksala et al. 2015), scaling the *TESS* data by a factor of 5 is sufficient.

Figure 1 shows the *TESS* light curve of σ Ori E, along with the rotational phase-binned light curve, and the best-fit model along with the associated continuum line. The best fit model has parameters $\beta = 70°$, $i = 63°$, $\tau_K = 3.6$, and $W = 0.21$. The primary eclipse is fit relatively well, with absorption and emission in both the model and *TESS* data occurring at the same phases. The large β associated

Table 1. Best-fit parameters for each star from the current work as well as from Shultz et al. (2019b). For the case of σ Ori E, Shultz et al. (2019b) assumed an inclination $i \sim 80°$ in accordance with Oksala et al. (2015). The Shultz et al. (2019b) revised row makes no assumptions about i and allows it to be a free parameter.

	$M_*(M_\odot)$	$R_*(R_\odot)$	B_*(kG)	β (°)	i (°)	W	τ_K, best-fit	τ_K, eq. 3
				σ Ori E				
Current Work	–	–	–	70^{+10}_{-1}	63^{+5}_{-1}	$0.21^{+0.29}_{-0.1}$	$3.6^{+0.4}_{-0.3}$	–
Shultz et al. (2019b)	$7.9^{+0.2}_{-0.3}$	$3.39^{+0.04}_{-0.06}$	10^{+2}_{-1}	38 ± 9	77 ± 4	$0.224^{+0.003}_{-0.004}$	$1.5^{+0.6}_{-0.3}$	$0.20^{+0.08}_{-0.04}$
Shultz et al. (2019b), revised	$8.3^{+0.6}_{-0.7}$	3.9 ± 0.6	9.6 ± 1.2	75^{+2}_{-10}	52 ± 7	$0.229^{+0.100}_{-0.003}$	$3.90^{+4.64}_{-0.98}$	$0.25^{+0.30}_{-0.06}$
				HD 142184				
Current Work	–	–	–	30 ± 1	58 ± 1	$0.10^{+0.05}_{-0}$	$4.0^{+0}_{-0.1}$	–
Shultz et al. (2019b)	5.7 ± 0.1	2.8 ± 0.1	9 ± 2	9 ± 3	64 ± 6	$0.524^{+0.064}_{-0.035}$	$1.00^{+0.55}_{-0.47}$	$1.49^{+0.82}_{-0.71}$
				HD 182180				
Current Work	–	–	–	84 ± 1	66 ± 1	0.40 ± 0.01	0.5 ± 0.1	–
Shultz et al. (2019b)	6.5 ± 0.2	3.2 ± 0.1	9.5 ± 0.6	82 ± 4	53^{+9}_{-5}	$0.562^{+0.068}_{-0.061}$	$0.80^{+0.27}_{-0.25}$	$2.30^{+0.79}_{-0.72}$
				HD 345439				
Current Work	–	–	–	25 ± 1	67 ± 1	$0.20^{+0.09}_{-0.06}$	$2.2^{0.3}_{-0.4}$	–
Shultz et al. (2019b)	8.3 ± 0.8	3.7 ± 0.5	8.9 ± 1.1	46 ± 13	59 ± 10	$0.407^{+0.093}_{-0.076}$	$3.2^{+2.1}_{-1.7}$	$0.89^{+0.58}_{-0.49}$

with our model fit exhibits "plateaus" of emission, rather than peaks. This complements well with what we see in σ Ori E, where phases between eclipses are characterized by flat-topped maxima. Indeed, these plateaus in the light curve of σ Ori E are not of equal length and height. This effect is produced by our model light curve, and supports the idea that the obliquity of σ Ori E's magnetic field may be higher than originally anticipated.

Another unexpected result of this analysis is the location of the continuum line with respect to the light curve of σ Ori E. Here, both phases between the eclipses are above the continuum line, which shows that a significant amount of electron scattering emission is occurring between eclipses. In previous analyses the continuum was assumed to be located at the level of the secondary maxima, which occurs at a flux level $\sim 2\%$ above the continuum. This then leads to a small amount of emission at phase ~ 0.6, which was originally picked out and the main point of motivation for the work done by Berry et al. (2022). With our best fit model we now show that more continuum emission may be present in the light curve of σ Ori E than first expected.

A key difference between our best-fit model here and results from previous literature is the inclination angle. Previous work showed that an inclination angle $i \geq 75°$ is required to reproduce the level of absorption seen with σ Ori E (Oksala et al. 2015). Instead, we produce here a best-fit light curve with $i = 63°$, considerably lower than what has been shown previously. Furthermore, the triangle plot of Figure 1 shows that inclination is fairly well constrained around $\beta = 60°$ within the 3σ confidence level.

W is a parameter that is well recovered for the case of σ Ori E. Our best fit value of $W = 0.21$ is in good agreement with Shultz et al. (2019b), who provide $W \approx 0.22$.

$\tau_K = 3.6$ here is quite high, but not surprising given the amount of absorption and emission required to match the levels seen in this particular light curve. Indeed, Berry et al. (2022) did predict that a best-fit light curve for σ Ori E would require τ_K to be around 2. With σ Ori E's $\sim$ 10 kG magnetic field and relatively small W we find here, Equation 3 gives $\tau_K = 0.2$, about a factor of 10 lower than the optical depth we need to reproduce the degree of photometric variation seen in this light curve.

Due to the large disrepancies in angular values, we also compare to a set of "revised" values calculated using the same method and priors as adopted by Shultz et al. (2019b), only now lifting the constraint on inclination which before was forced to be as close to 85° as possible in accordance with Oksala et al. (2015). Inclination is now free to vary, resulting in differing values for other parameters, most notably β which is now much larger than previously reported by Shultz et al. (2019b) (see Table 1).

The forward modeled light curve in Figure 1 has parameters from the Shultz et al. (2019b) revised row of Table 1, which are in better agreement with those of our best-fit model than those from the literature. The forward modeled curve has high obliquity and a relatively low W, which results in the plateaued peaks seen in our best-fit model as well as in the data. However, the empirical light curve is not well-fit by the forward modeled light curve, and this is due to the moderate inclination $i = 52°$. If it were higher, around $i = 63°$ of the best-fit model, then the data would likely be better fit.

4.2 HD 142184

HD 142184 is a B2V star with a $\sim 10-15$ kG magnetic field (Grunhut et al. 2012a) with a more recent calculation finding a weaker field of $\sim$ 9 kG (Shultz et al. 2019b). It has the most rapid rotation of any known magnetic early B-type star to date with a period of $0.508275^{+0.000015}_{-0.000012}$ days (Grunhut et al. 2012a). With a strong magnetic field and rapid rotation, this star is likely to host a CM. Indeed the strong Hα emission supports this (Grunhut et al. 2012a). Grunhut et al. (2012a) infer red a viewer inclination $i \sim 70 \pm 10°$. The magnetic field is marginally oblique with $\beta \sim 10°$ (Grunhut et al. 2012a; Shultz et al. 2019b). Other effects such as gravity darkening and oblateness from rapid rotation could have small effects on photometric variation from this star (Grunhut et al. 2012a). Via visual comparison of the *MOST*

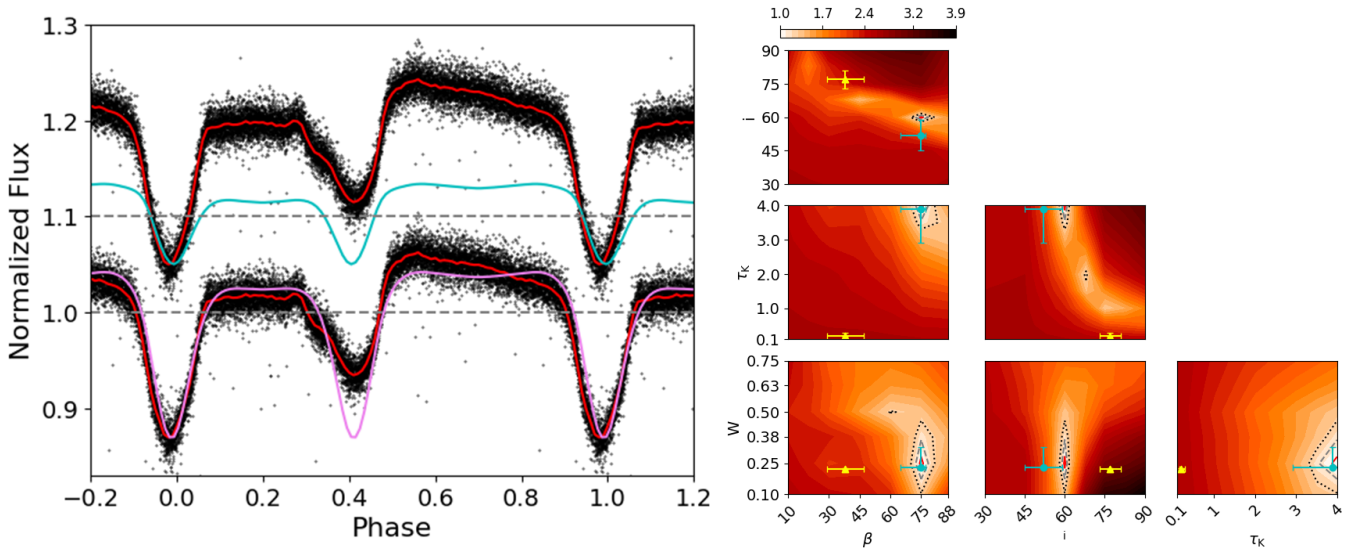

Figure 1. *Left*: *TESS* light curve of σ Ori E (black points) with the 100 point binned light curve (red) overlaid with our best fit model (purple) and the forward modeled light curve from minimally constrained parameters (cyan; Shultz et al. 2019b). The best fit model has parameters $\beta = 70°$, $i = 63°$, $\tau_K = 3.6$ and $W = 0.21$. The forward modeled curve has parameters $\beta = 75°$, $i = 52°$, $\tau_K = 3.9$ and $W = 0.229$ and has been shifted arbitrarily in flux for clarity. The dashed grey line is the continuum flux, i.e. the flux from the star if there were no magnetosphere present, or if the magnetosphere were optically thin. *Right*: Contour plots showing log reduced χ^2 in each plane within the parameter space. Brighter areas are associated with a reduced χ^2 closer to 1, and a better fit. log σ confidence levels are shown as contour lines with 1σ (solid red), 2σ (dashed grey) and 3σ (dotted black). Values and errors directly from Shultz et al. (2019b) are shown as the yellow triangles, and values found from a minimally constrained calculation are shown as the cyan points. τ_K is calculated from Equation 3 for the yellow triangles, but is a free parameter for the cyan points.

light curve to the photometric RRM models developed by Townsend (2008), they argued that the magnetosphere is the main cause of this star's light curve morphology.

Figure 2 shows the *MOST* light curve (black points) with the binned light curve fitted with our best-fit model (purple) with parameters $\beta = 30°$, $i = 58°$, $\tau_K = 4$ and $W = 0.1$. To start, our best-fit model predicts W considerably lower than the value determined from the star's rotation period, mass, and radius. The light curve of HD 142184 contains only one apparent eclipse. This is consistent with the Hα emission which Grunhut et al. (2012a) noted is asymmetrical and displays only one eclipse, they further observed that the light and Hα equivalent width curves followed one another very closely. Our oblique models always contain two main clumps of material, which leads to double eclipsing. However, with certain combinations of our four parameters, it is possible for the stellar disk to be occulted only once by the magnetosphere. One substantial eclipse can occur at low obliquity, moderate inclination, low W and higher τ_K (figure 8 of Berry et al. 2022), which we see here.

We recover the low obliquity with our best-fit model, though it is larger than $\beta \approx 10°$ obliquity predicted by Shultz et al. (2019b). However, the triangle plot of Figure 2 shows that β is highly constrained around $\beta = 30°$.

We recover the moderate inclination angle predicted by Grunhut et al. (2012a) and Shultz et al. (2019b), despite it being a bit shallower than expected. i is highly constrained on the triangle plot of Figure 2 around $i = 53°$

$\tau_K = 4$ for our best-fit model is very large for a continuum optical depth, even for the most rapidly rotating star known. However, it is possible for a CM to become this optically thick in the continuum for a star with $W \approx 0.5$, as long as the surface polar magnetic field strength $B_* \approx 15$ kG. The initial prediction for the presence of a $10-15$ kG magnetic field made by Grunhut et al. (2012a) means that such an optical depth for HD 142184 could be possible, but more recent results by Shultz et al. (2019b) found $B_* = 9 \pm 3$ kG. This brings down the largest possible optical depth down to around 2.

Another interesting result from HD 142184 is the location of the continuum flux with respect to the light curves. Our best-fit model shows that the flux is always $\sim 10\%$ above the continuum flux solely due to magnetospheric emission. Due to both τ_K and W being considerably different from the literature values, this is likely not true in reality.

Despite having parameters much closer to their inferred value, the forward modeled light curve for HD 142184 does not give a good fit. Because of the low obliquity, moderate inclination and high W, the magnetosphere spends most of the time in phase in front of the star, which then leads to wide eclipses and a single rounded peak. This is the opposite of what we see in the data, where one short eclipse is present, followed by a large plateau. However, the best-fit $\tau_K = 1$ in the forward modeled light curve is much more reasonable than the $\tau_K = 4$ associated with our best-fit model, while producing the same levels of absorption seen in the *MOST* data. The smaller τ_K also results in a single rounded peak of emission above the continuum flux.

4.3 HD 182180

HD 182180 is a B2V helium-rich star known to host a strong ($\sim$ 10 kG) oblique dipolar magnetic field ($75 \pm 10°$, $82 \pm 4°$; Rivinius et al. 2013; Shultz et al. 2019b, respectively), and is one of the fastest rotators known with a period of 0.521428 ± 0.000006 days (Oksala et al. 2010; Rivinius et al. 2008, 2010; Rivinius et al. 2013). Due to the presence of a strong magnetic field and fast rotation, HD 182180 should most likely host a centrifugal magnetosphere, and this is supported by the presence of strong Hα emission (Rivinius et al. 2013). Furthermore, the combination of a strong magnetic field and fast rotation gives a continuum optical depth of order unity,

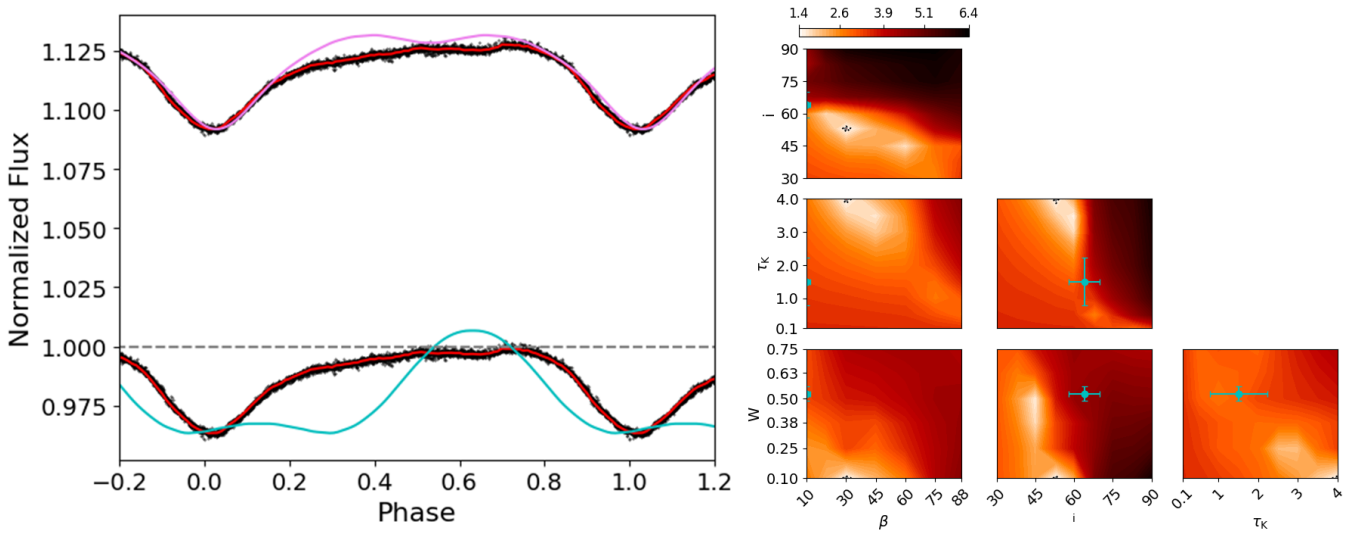

Figure 2. *Left*: *MOST* light curve of HD 142184 (black points) with the 100 point binned light curve (red) overlaid with our best fit model (purple) and the forward modeled light curve from minimally constrained parameters (cyan; Shultz et al. 2019b). The best fit model has parameters $\beta = 30°$, $i = 58°$, $\tau_K = 4$ and $W = 0.1$. The forward modeled curve has the same parameters provided by Shultz et al. (2019b) with a best-fit $\tau_K = 1$. The dashed grey line is the continuum flux, i.e. the flux from the star if there were no magnetosphere present, or if the magnetosphere were optically thin. *Right*: Contour plots showing log reduced χ^2 in each plane within the parameter space. Brighter areas are associated with a reduced χ^2 closer to 1, and a better fit. log σ confidence levels are shown as contour lines with 1σ (solid red), 2σ (dashed grey) and 3σ (dotted black). Values and errors from Shultz et al. (2019b) are shown as the cyan points. τ_K is calculated from Equation 3.

which should provide a small but significant amount of electron scattering emission. The expected large viewer inclination angle, combined with a high magnetic obliquity and a relatively optically thick magnetosphere means that the amount of photometric variation in the light curve of HD 182180 may be due to magnetospheric absorption and scattering. HD 182180 is known to have sources of variability other than the magnetosphere, such as surface abundance spots (Oksala et al. 2010; Rivinius et al. 2013). Other effects such as gravity darkening and oblateness from rapid rotation may have small effects on the photometric variation for this particular star (Rivinius et al. 2013).

The left panel of Figure 3 shows the *K2* light curve of HD 182180 over-plotted with our best-fit model (purple) with parameters $\beta = 84°, i = 66°, \tau_K = 0.5$ and $W = 0.4$. The fit matches the depth of the primary eclipse well, and matches both minima and maxima in the light curve in phase. The model overestimates the depth of the secondary eclipse. This is a consequence of the tilted dipolar magnetic field topology adopted in our models - both eclipses will have the same depth as the plasma distribution in the magnetosphere is symmetrical across the magnetic field axis. Another difference between the data and our models are the rounded peaks of HD 182180's light curve, contrasted with the "plateaus" in our model. These plateaued peaks are an effect seen with large β (see Figures 7 and 8 of Berry et al. 2022), as well as with slower rotation speeds, as the magnetosphere will spend more time off the limb of the stellar disk. In any case, the obliquity of HD 182180's magnetic field and its rotation speed are both known to be quite high, which is in good agreement with our values for β and W (Rivinius et al. 2008; Oksala et al. 2010; Shultz et al. 2019b).

The viewer inclination $i = 66°$ obtained from our best fit model is in good agreement with values derived elsewhere (Rivinius et al. 2008; Oksala et al. 2010; Shultz et al. 2019b). Inclination for this star is highly constrained around $i = 66°$ by our models, according to the triangle plot in the right panel of Figure 3.

Another discrepancy between the data and our best-fit model is that the primary eclipse width is not exactly matched. This is likely due our best-fit model having a smaller W than expected, which results in skinnier eclipses. Indeed, the forward modeled light curve, which has a higher $W = 0.56$, does fit the primary eclipse width better than our best-fit model, but does not match the secondary eclipse nearly as well.

τ_K, however, is a parameter that remains difficult to predict. Using values for the magnetic field and rotation speed provided by Shultz et al. (2019b), ($B_* = 9.5$ kG, $W = 0.56$) as well as the stellar mass and radius gives an associated $\tau_K \approx 2.3$. However, our best fit model has $\tau_K = 0.5$, which undercuts this calculated value by a factor of ~ 5, and is rather unexpected given the strong magnetic field and fast rotation speed associated with this star. In fact, this is the opposite problem that we have seen for σ Ori E, in which the predicted τ_K is higher than the calculated value. Here, the predicted τ_K is lower than what we calculate from Equation 3. We are unlikely to find a good fit higher or lower than $\tau_K = 0.5$. The triangle plot of Figure 3 shows that τ_K is highly constrained to 0.5 within the three σ confidence levels.

Another surprising result from our best-fit model is the location of the continuum line with respect to the observations. When looking at the light curve for HD 182180, it's quite clear to see that magnetospheric emission could be present, mainly due to the rounded peaks of this particular light curve. Photometric emission is also expected from the strong Hα emission. However, our best fit model shows that no amount of emission above the continuum flux is present.

The forward modeled light curve in cyan is a reasonable fit, which is unsurprising given the similarity between our best-fit parameters and the values provided by Shultz et al. (2019b). The main difference between the forward modeled light curve and our best-fit is the presence of emission in the former. This is likely due to a smaller i, larger τ_K and larger W. However, the forward modeled light curve does not match the secondary eclipse and peak width and depth, which is likely a result of larger W and smaller i.

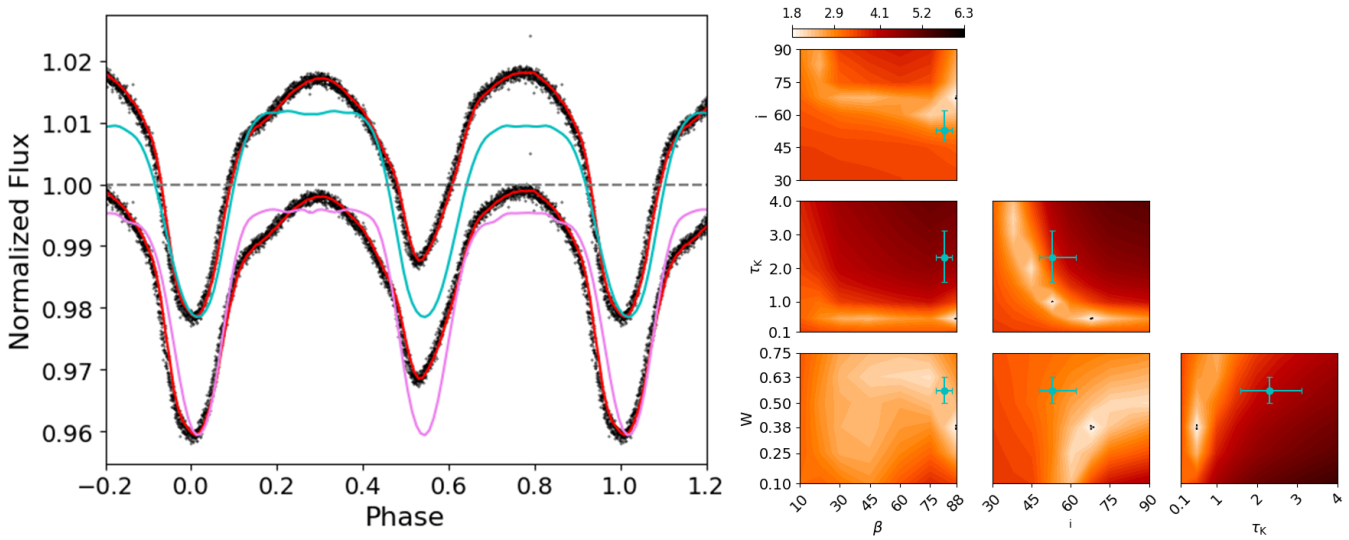

Figure 3. *Left*: *Kepler* light curve of HD 182180 (black points) with the 100 point binned light curve (red) overlaid with our best fit model (purple) and the forward modeled light curve from minimally constrained parameters (cyan; Shultz et al. 2019b). The best fit model has parameters $\beta = 84°$, $i = 66°$, $\tau_K = 0.5$ and $W = 0.4$. The forward modeled curve has the same parameters provided by Shultz et al. (2019b), with a best-fit $\tau_K = 0.8$. The dashed grey line is the continuum flux, i.e. the flux from the star if there were no magnetosphere present, or if the magnetosphere were optically thin. *Right*: Contour plots showing log reduced χ^2 in each plane within the parameter space. Brighter areas are associated with a reduced χ^2 closer to 1, and a better fit. log σ confidence levels are shown as contour lines with 1σ (solid red), 2σ (dashed grey) and 3σ (dotted black). Values and errors from Shultz et al. (2019b) are shown as the cyan points. τ_K is calculated from Equation 3.

4.4 HD 345439

HD 345439 is a rapidly rotating B2V star known to host a strong (~ 12 kG; Hubrig et al. 2015, 2017) magnetic field with a rapid rotational period of ~ 0.77 days, comparable to the rotation period of HD 142184 and HD 182180 (Wisniewski et al. 2015). Due to the presence of a strong magnetic field and rapid rotation, this star is capable of hosting a CM. Spectroscopy of this star presented by Wisniewski et al. (2015) shows that the equivalent widths of multiple emission and absorption lines are phase dependent. Specifically, periodic behavior of the star's double-peaked Hα emission indicates that a CM exists around HD 345439, as originally inferred by Eikenberry et al. (2014) on the basis of the similar morphology of the star's Brackett lines. Wisniewski et al. (2015) suggest that photometric variability of HD 345439 is due in most part to a co-rotating magnetosphere, but do not rule out the possibility that pulsations have an effect on the light curve morphology.

However, the higher-quality *TESS* light curve was examined by Jayaraman et al. (2022), who suggested that its variability was likely entirely consistent with the presence of a CM. Wisniewski et al. (2015) noted that detailed modeling should be done for HD 345439, and suggested that this system should have a high inclination ($i \sim 75°$) and a moderate magnetic obliquity ($\beta \sim 45°$) based on photometric RRM light curves presented by Townsend (2008). Spectropolarimetric and evolutionary modelling by Shultz et al. (2019b) found $i = 59 \pm 10°$, $\beta = 46 \pm 13°$, and $B_d = 9 \pm 1$ kG, consistent with the predictions of Wisniewski et al. (2015) and Hubrig et al. (2017).

Figure 4 shows the *TESS* light curve along with our best-fit model in purple, with parameters $\beta = 25°$, $i = 67°$, $\tau_K = 2.2$ and $W = 0.2$. The fit matches the overall morphology of this light curve quite well, with the levels of emission and absorption occurring at the same level and time in phase. This particular light curve exhibits two maxima of highly unequal fluxes, with one maximum below the grey dashed continuum line, and one above. This effect in the model is most likely due to the fact that the magnetosphere is still occulting part of the stellar disk when the magnetic field axis is pointing away from the observer, an effect from the relatively low β and W.

The primary maximum of the light curve of HD 345439 displays a "plateaued" peak, similar to those seen in the light curve of σ Ori E. This feature is somewhat matched by our model, though the duration of the plateau does not last as long in phase as it does in the *TESS* data. The secondary maximum of the observations also displays a plateaued peak. This is not matched by the secondary maximum of our best-fit model, which exhibits a rounded peak. The length of these plateaus can be increased by increasing β or by decreasing W. W is already quite small, so it's unlikely that it should be decreased. A larger β may be in order in accordance with $\beta \approx 45°$ as Wisniewski et al. (2015) and Shultz et al. (2019b) have suggested.

However, increasing β will also have the effect of increasing the flux of the secondary maximum, which would most likely lead to an overestimation of the secondary maximum seen for HD 345439. Furthermore, the triangle plot of Figure 4 shows that β is highly constrained around $\beta = 25°$. However, W is less constrained with a range of $0.1 \lesssim W \leq 0.25$ within the 3σ confidence level. This shows that it is certainly possible for W to be somewhat larger, which would be in better agreement with the value of $W = 0.4 \pm 0.1$ found by Shultz et al. (2019b).

Inclination $i = 67°$ agrees well with values found by Wisniewski et al. (2015) and Shultz et al. (2019b). The triangle plot of Figure 4 shows that inclination for this star is tightly constrained around $i = 67°$.

The optical depth $\tau_K = 2.2$ for our best-fit model is reasonable, given the amount of absorption and emission required to reasonably fit the light curve of HD 345439. The associated $\tau_K = 0.9$ is calculated from Equation 3 using values pulled directly from Appendix C of Shultz et al. (2019b). The triangle plot of Figure 4 shows that τ_K is fairly constrained, with a range $2 \lesssim \tau_K \lesssim 2.5$ within the 3σ confidence level.

The location of the continuum flux (grey dashed line) with respect

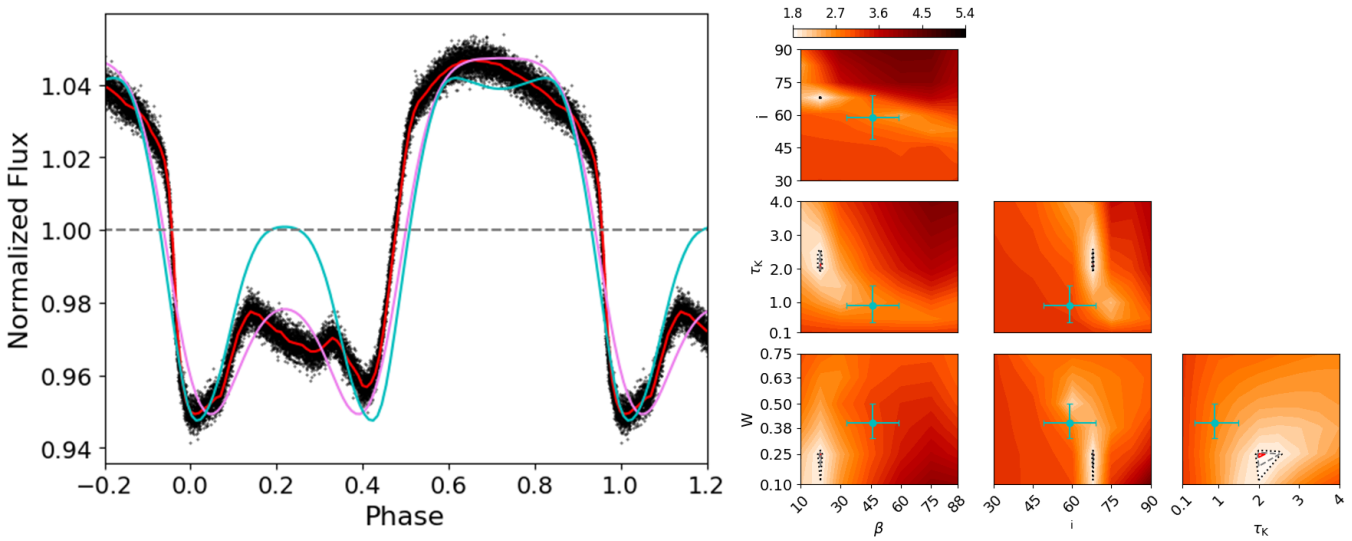

Figure 4. *Left*: *TESS* light curve of HD 345439 (black points) with the 100 point binned light curve (red) overlaid with our best fit model (purple) and the forward modeled light curve from minimally constrained parameters (cyan; Shultz et al. 2019b). The best fit model has parameters $\beta = 25°$, $i = 67°$, $\tau_K = 2.2$ and $W = 0.2$. The forward modeled curve has the same parameters provided by Shultz et al. (2019b), with a best-fit $\tau_K = 3.2$. The dashed grey line is the continuum flux, i.e. the flux from the star if there were no magnetosphere present, or if the magnetosphere were optically thin. *Right*: Contour plots showing log reduced χ^2 in each plane within the parameter space. Brighter areas are associated with a reduced χ^2 closer to 1, and a better fit. log σ confidence levels are shown as contour lines with 1σ (solid red), 2σ (dashed grey) and 3σ (dotted black). Values and errors from Shultz et al. (2019b) are shown as the cyan points. τ_K is calculated from Equation 3.

to the light curves shows that there is a significant level of magnetospheric emission occurring around HD 345439, with ~ 4% extra emission from magnetospheric scattering.

The forward modeled light curve for this star is quite similar in structure to our best-fit model, with the main differences being a result of a larger β and W than our best-fit. $\beta = 46°$ results in a higher and wider secondary peak. Meanwhile, the larger W results in a slightly skinnier absolute maximum. $\tau_K = 3.2$ in the forward modeled light curve is even larger than the best-fit model. However, given the smaller i and larger W than in the latter, a larger τ_K in the former is needed to match the levels of absorption and emission in the *TESS* light curve.

5 DISCUSSION

Our aim in this work is to do a blind test on a sample of stars, using only the available photometry, along with models presented by Berry et al. (2022) and expanded upon here in order to infer magnetic and rotational properties of these stars. Parameters inferred from the photometric analysis are then compared to those independently determined by Shultz et al. (2019b) via spectroscopic measurements of atmospheric parameters, direct spectropolarimetric measurements of the surface magnetic field, rotational periods and projected rotation velocities, and stellar parameters inferred from evolutionary models. We show that the photometric RRM models, which assume a purely dipolar magnetic field topology, can reasonably recover three out of the four parameters for most stars, except for HD 142184. This has important implications, as we show that even the simplest models we use here can reasonably fit these stars' light curves, which can be useful in cases where a star's magnetic and rotational properties cannot be reliably measured.

5.1 Comparison to Previous Results

Figure 5 shows our best-fit values for each parameter versus those determined by Shultz et al. (2019b). To start, there is good agreement in β, especially for HD 182180 and the σ Ori E revised values; though for most stars we predict higher β than Shultz et al. (2019b). One reason for this discrepancy is the plateaued peaks which occur in the light curves of all stars other than HD 182180. The presence of plateaued peaks, rather than rounded peaks is a signature of large β in the models presented by Berry et al. (2022). The only exception to this discrepancy is HD 345439, in which we underestimate β as compared to the value given by Shultz et al. (2019b). Indeed, a larger β would result in a longer plateau for this star's absolute maximum. However, increasing β also raises the secondary maximum as seen by the cyan curve in Figure 4. β also has a slight effect on eclipse width, with eclipses becoming sharper with increasing β.

Strong agreement in i exists between our models and the values provided by Shultz et al. (2019b). This is expected, as a large inclination is required to produce any noticeable photometric variation (Townsend 2008; Berry et al. 2022). In order to recover the double eclipsing seen in each star here, with the exception of HD 142184, a combination of i and β must exist such that $i + \beta \gtrsim 90°$ (Townsend 2008). This condition is met by our models as well as with values from Shultz et al. (2019b) for all stars other than HD 142184, which helps explain why that star only shows one clear eclipse.

W is reliably recovered, except for HD 142184, though our models tend to be lower than the values given by Shultz et al. (2019b). In general, W controls eclipse depth and eclipse width, as well as controlling the width of emission peaks. W also has a weak effect on the level of emission (Berry et al. 2022). Once again, the light curves for stars other than HD 182180 show prominent plateaued peaks, which, as well as being a sign of lower β, is an effect of low W. Furthermore, larger W will lead to wider eclipses, which can last ~ 0.2 in phase for $W \geq 0.5$ (Berry et al. 2022). However, eclipses in

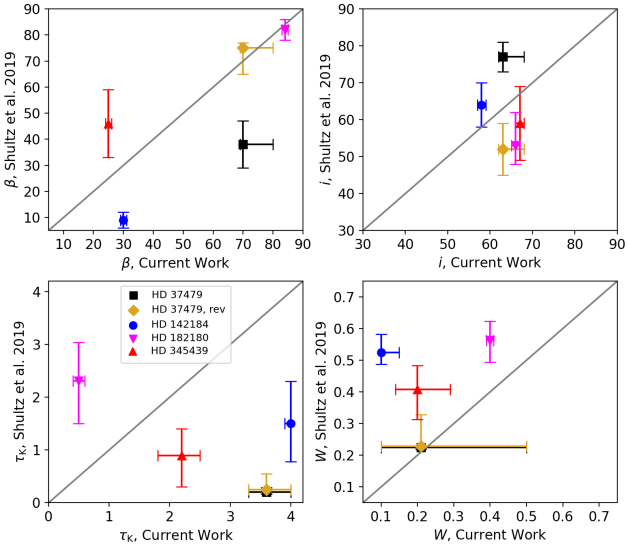

Figure 5. β, i, τ_K, and W comparisons between our best-fit models and values found by Shultz et al. (2019b), and listed in Table 1. τ_K is calculated from Equation 3. The closer each point is to the grey line, the better the agreement.

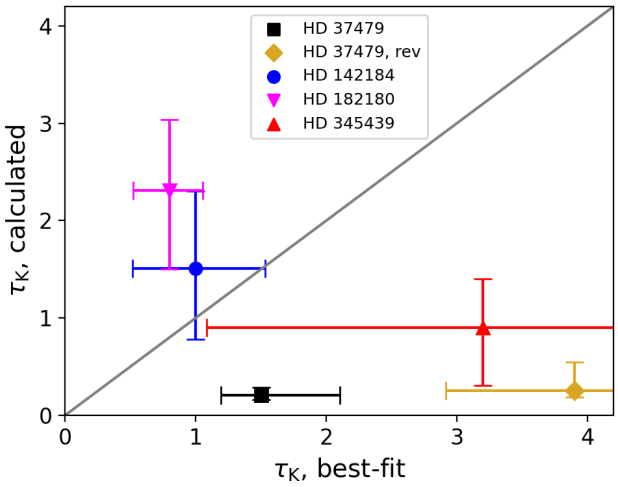

Figure 6. Calculated τ_K from Equation 3 versus best-fit τ_K using the forward modeled light curves from Shultz et al. (2019b), with the associated parameters listed in Table 1.

each of these stars do not last that long in phase, which in our models is indicative of smaller W.

The one parameter we cannot reliably recover is τ_K. We use Equation 3 to predict what τ_K should be given M_*, R_*, B_* and W. Despite this, we do not reliably recover τ_K using our models. This was an issue first brought up in the discussion by Berry et al. (2022), in which they noted that $\tau_K \sim 2$ would be needed to match the levels of photometric variation seen in the light curve of σ Ori E. However, using the same expression as Equation 3, Berry et al. (2022) found $\tau_K \approx 0.21$, which would not nearly match the light curve amplitude of σ Ori E. This discrepancy is seen here again with σ Ori E even more-so, as our best-fit model predicts $\tau_K = 3.6$. Furthermore, Equation 3 underestimates the best-fit τ_K for HD 345439 and HD 142184 as well. Oddly enough, Equation 3 *overestimates* τ_K given by our best-fit model for HD 182180.

Possible causes of these discrepancies are discussed by Berry et al. (2022). One possibility has to do with the correction factor c_f assumed to be 0.3 by Owocki et al. (2020) based on calibration by 2D MHD, which may be incorrect for oblique models. For the case of σ Ori E, Berry et al. (2022) found that c_f needs to be of order unity. Doing the same thing for HD 345439 and HD 142184 using the best-fit τ_K from our models and associated M_*, R_*, B_* and W from Shultz et al. (2019b), we again find that c_f needs to be of order unity. Having c_f be order unity, however, would not solve the overestimation in calculated τ_K for HD 182180. In order to get a calculated $\tau_K \approx 0.5$, $c_f \sim 10^{-2}$ is needed, an order of magnitude smaller than the value inferred by Owocki et al. (2020). The main difference between HD 182180 and the other stars in this analysis is the extremely high obliquity of $\beta \sim 80°$. This leads us to propose that c_f may be a function of β that does not monotonically increase.

Another factor which could play a role in determining τ_K is the star's effective temperature, $T_{\rm eff}$. Figure 6 shows τ_K according to Equation 3 versus the best-fit τ_K. For σ Ori E and HD 345439, Equation 3 underestimates the best-fit τ_K. However, for HD 142184 and HD 182180, Equation 3 *overestimates* the best-fit τ_K. The main difference between these two groups of stars is their $T_{\rm eff}$. Specifically, HD 142184 and HD 182180 are cool for their spectral type ($T_{\rm eff} \approx 17$ kK for both stars; Grunhut et al. 2012a; Rivinius et al. 2013), while σ Ori E and HD 345439 are hotter ($T_{\rm eff} = 23 \pm 2$ kK for both stars; Shultz et al. 2019a). $T_{\rm eff}$ plays a direct role in a star's mass loss rate, with cooler stars having less powerful winds, resulting in an overall less dense and less optically thick CM.

$T_{\rm eff}$ plays a role in CBO-regulated mass transport (Shultz et al. 2020; Owocki et al. 2020). Specifically, as $T_{\rm eff}$ decreases, leakage as a means of mass transport becomes a more prominent process, and breakout events become less common. If leakage becomes the dominant process, then it's possible that the CM can never reach its breakout density, hence limiting τ_K, and making it more difficult to maintain an optically thick CM.

The ultimate discrepancy between our models and the data is the fact that our models use a purely dipolar magnetic field. There are no contributions from higher order multipoles. This leads to symmetry in our models, in which the two clouds of material in the CM are essentially mirrored about the magnetic field axis. This in turn leads to symmetries in our model light curves which are not present in the observed light curves (see figures 7 and 8 of Berry et al. (2022), in which every light curve is mirrored about phase 0.5). Such symmetry is not seen in any of data, with light curves having different eclipse depths and rounded or plateaued peaks. HD 142184 has only one eclipse in both the continuum and Hα when we would expect it to have two based on its geometric properties. σ Ori E is the only star in this analysis that we know does not have a purely dipolar magnetic field topology (Oksala et al. 2015; Krtička et al. 2022). However, asymmetries in Hα emission bumps seen in each star here (Oksala et al. 2012; Grunhut et al. 2012a; Rivinius et al. 2013; Wisniewski et al. 2015) points to the presence of more complex magnetic field topologies than a pure dipole.

Despite this, we can still reliably recover 3 of the 4 parameters, as well as reasonably fit these stars' light curves. This has important implications. To start, tilted dipoles are by far the simplest topology to model, and makes the fewest assumptions. Complex magnetic field topologies can only be reliably measured using high-resolution spectropolarimetric time series, which are difficult to obtain for extremely rapidly rotating stars, especially for those which are dim (e.g. with V magnitudes ≥ 8, one of which is HD 345439 with Vmag =

11.11; Høg et al. 2000). This means that for certain stars, we can only reliably depend on photometry to infer their rotational and magnetic properties.

Photometric variation from CM's governed by higher order multipoles has been investigated by Krtička et al. (2022), who found that the rigidly rotating magnetosphere model can explain tiny features in light curves only when higher order multipoles dominate the magnetic field out to R_K. Krtička et al. (2022) considered multipoles up to order $n = 9$, with combinations of magnetic field topologies considered as well. Similar physics to those employed by Berry et al. (2022) were used to simulate light curves with both magnetospheric absorption and electron scattering emission.

However, one key difference is that Krtička et al. (2022) simplified radiative transfer to make it less computationally expensive to solve. Specifically, Krtička et al. (2022) assumed that light only reflects off the surface of the clouds, with any emission inside the clouds ignored. Krtička et al. (2022) found this approximation to be acceptable. However, the RRM models developed by Berry et al. (2022) and used in this work fully solve the radiative transfer equation using a scattering source function, which means that emission throughout the whole magnetosphere is considered. Furthermore, Krtička et al. (2022) adopt a density scaling $\rho \sim r^{-3}$, the same scaling introduced by Townsend & Owocki (2005) which is based on the magnetosphere filling time. This leads to a slower decrease in density and overall less dense magnetosphere. The model presented by Berry et al. (2022) and again used here use recent CBO scalings (Owocki et al. 2020) which have density scale like $\rho \sim r^{-5}$. This leads to a sharper decline in density, but makes the magnetosphere overall more dense than the r^{-3} scaling. Our models also take recent MHD simulations (ud-Doula 2021) into account, thus motivating the introduction of χ, which controls the azimuthal distribution of density.

Varying χ was not explored by Berry et al. (2022) or in the present work, though it is not difficult to infer how the morphology of our models would change with respect to variation of χ. To reiterate, $\chi = 0.05$ in all of our models. As defined by Equation 2, if we wanted to increase the azimuthal distribution of density in the magnetosphere, we would need to increase χ. This would decrease the plateauing we see in models with high β and low W, perhaps leading to better fits for stars such as HD 182180. Increasing χ should also increase the amount of absorption, especially at high β. Decreasing χ has the opposite effect; material will now become more confined to the common magnetic-rotational equator, where there is the greatest centrifugal support. This will increase the plateauing, meaning longer plateaus even at lower β. As such, decreasing χ could perhaps lead to better fits for σ Ori E and HD 345439. Decreasing β should also have the effect of decreasing the amount of absorption.

The light curve of σ Ori E was fit by Krtička et al. (2022), using a magnetic field with a combination of a dipole and a quadrupole. Magnetospheric absorption and emission was taken into account, as well as surface spots from Oksala et al. (2015). This fit is much better than that shown in this work. Both eclipses are well fit due to the introduction of quadrupole contributions, whereas we overestimate the secondary eclipse by about 5%. However, while we do see an emission bump in the model present by Krtička et al. (2022), it does not match the morphology of the inferred emission bump which occurs at phase $\sim$ 0.6. Furthermore, Krtička et al. (2022) adopt $\beta = 90°$ for their model fit, even larger than our best-fit $\beta = 70°$.

5.2 Application to other σ Ori E variable Stars

In order to illustrate the relatively comprehensive nature of this study, Fig. 7 shows the logarithmic strength of the equatorial magnetic field at the R_K as a function of the rotational axis inclination angle i for stars with Hα emission characteristic of line formation in a centrifugal magnetosphere. The majority of the stars were taken from the sample examined by Shultz et al. (2020), with two subsequently discovered additions (HD 156424B, Shultz et al. 2021b; and W 601B, Shultz et al. 2021a). Symbol size is proportional to Hα emission equivalent width (EW), i.e. the difference between the observed and synthetic photospheric Hα profile at the rotational phase of maximum emission strength; this quantity serves as a proxy for the size of the magnetosphere, and as discussed by Shultz et al. (2020) has been corrected for dilution in the case of spectroscopic binaries.

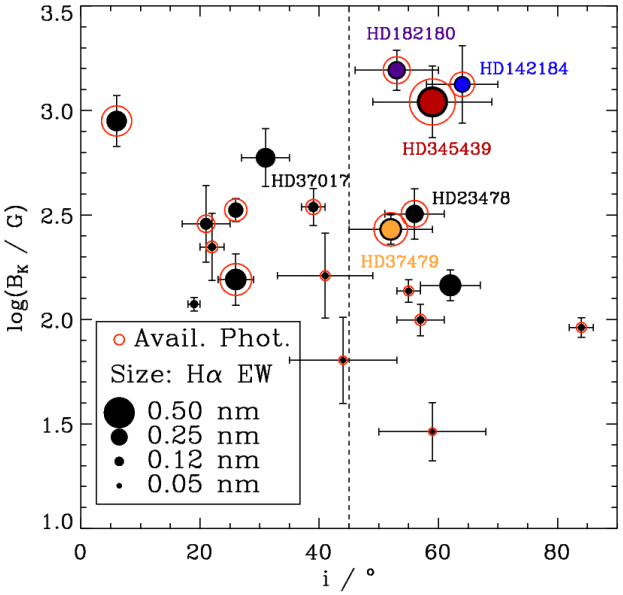

Figure 7. log B_K as a function of the inclination angle for stars with CM-type Hα emission. As indicated in the legend, symbol size is proportional to Hα emission EW, and outlined symbols indicate stars with available space photometry. Stars studied in this work are highlighted and labeled. Other labeled stars are discussed in the text. The vertical dashed line indicates the approximate lower limit in inclination for eclipsing.

The vertical dashed line at $i = 45°$ indicates the approximate lower limit for stars to be eclipsed by their CMs. Of those stars with large magnetospheres as inferred from their Hα emission, only 6 are above this limit. For one, HD 164492C, space photometry is not available (and is likely to be difficult to interpret if it does become available, as this is a dim star in a very crowded field; Wade et al. 2017). Another, HD 23478, has strong Hα emission and an available *TESS* light curve, which has been examined by Jayaraman et al. (2022) and shows signs of magnetospheric influence. However, its Hα emission shows very low levels of variability (Sikora et al. 2015; Shultz et al. 2020), which is consistent with the very small β angle (about 6°) inferred from its magnetic field measurements (Sikora et al. 2015; Shultz et al. 2019b). Since little variation is expected in the light curve as a result of its magnetosphere, it is possible that much of the variability originates with photospheric spots, and we therefore chose to leave it out of the analysis; however, it should certainly be studied in future. The present study therefore includes the best 4 of the available 6 candidates.

Recent preliminary analysis of *TESS* light curves of magnetic chemically peculiar stars by Mikulášek et al. (2020) shows that several objects have "warped" light curves, characterized by a large number of harmonics. These light curves could not be fully repro-

duced via chemical spot models. These stars have parameters predicting large CMs (e.g. Shultz et al. 2019b) and have Hα emission properties consistent with this expectation (Shultz et al. 2020).

One such star is HD 37776. The main reason why this star could not be analyzed here is the fact that this star is known to host a magnetic field with complex multipolar topology (Kochukhov et al. 2011). As such, attempting to infer this star's magnetic and rotational properties using our dipolar models would be inappropriate. Furthermore, most of the photometric variation is due to surface spots (Krtička et al. 2007). This star was analyzed by Krtička et al. (2022), who used surface spots as well as an absorbing and emitting magnetosphere dominated by an octupolar magnetic field. Krtička et al. (2022) found that the presence of this magnetosphere accounted for subtle features in this light curve's morphology. While the light curves analyzed here could be reproduced with purely magnetospheric models. it's likely that the majority of stars with CMs – which tend to have weaker Hα emission and, presumably, less circumstellar material – will require simultaneous modelling of surface chemical abundances and magnetospheres in order to reproduce their light curves.

Another star which could be analyzed in the future is HD 37017. This star is not expected to produce eclipses due to its fairly shallow inclination $i = 38°$ and magnetic obliquity $\beta = 56°$ (Shultz et al. 2019b, ; see also Fig. 7). Indeed, there is no sign of eclipses in Hα (Shultz et al. 2020). However, Hα also shows that only one cloud may be present in the magnetosphere (Shultz et al. 2020), which is indicative of complex magnetic field topology. Alternatively, this highly asymmetric cloud structure is reminiscent of the that seen in the tidally locked binary system HD 156324, in which the gravitocentrifugal accumulation surface of the CM is warped by the orbital Roche geometry (Shultz et al. 2018a). Since HD 37017 is also a short-period binary (Bolton et al. 1998), it's magnetospheric geometry might also be affected by the gravitational influence of the companion. However, in contrast to HD 156324, HD 37017's orbit is eccentric, and the star's rotation is not synchronized with the orbital period; if there is an orbital influence, time-independent RRM models may prove inappropriate.

In general, stars suspected or confirmed of having large $\beta \sim 90°$ should be focused on in future studies. HD 182180 is the only star in the current work which is known to have high magnetic obliquity, a condition that we recovered. Since this star was the only example of Equation 3 overestimating the best-fit τ_K, other stars with large β should be analyzed to see if this phenomena is a trend for these stars, or an anomaly in the case of HD 182180.

6 SUMMARY AND FUTURE WORK

We've used RRM-CBO models from Berry et al. (2022) and applied them to a sample of stars: σ Ori E, HD 182180, HD 345439 and HD 142184. This model assumes a purely dipolar magnetic field, where all stars in this analysis have some contributions from higher order multipoles. Despite this, we find that we can reliably infer magnetic and rotational properties of σ Ori E, HD 182180 and HD 345439 with this simple model. We cannot reliably infer the magnetic and rotational properties of HD 142184, as our best-fit model includes a rotation speed that is far too slow, as well as a τ_K that is too large. This discrepancy is likely to HD 142184 having a more complex magnetic field topology than the other three stars. We note that τ_K remains difficult to predict, and suggest that the correction factor may be a function of β and/or $T_{\rm eff}$, based on the forward modeling. Future work can include:

- Models grounded in the same physics here can be made with varying χ to possibly better fit light curves of the four stars analyzed here, as well as others.
- The RRM-CBO model here should be updated to be able to model higher order multipoles; at least quadrupoles to start.
- Scattering is only one form of emission than can occur in CMs. Other forms of emission, such as Hα should be considered as well.
- Magnetohydrodynamic (MHD) simulations are another way to model magnetospheres. The RRM model used here adopted new scalings based on MHD simulations, one of which is the correction factor c_f, which we alluded may be a function of β. MHD simulations with highly oblique magnetic fields should be run to test this idea.
- The models shown here, as well as any future models involving higher order multipoles should be considered along with surface abundance spots to ensure the best fit for these light curves.
- Finally, the arbitrary rigidly rotating magnetosphere (ARRM) can be used to model oblique magnetic fields of higher order than dipoles. However, ARRM is limited, and often not an option in most cases.

Despite the models we present being relatively simple, we can still reliably recover β, i and W for HD 37479, HD 182180 and HD 345439. Therefore analyses similar to what we've done here could be useful for stars for which spectropolarimetry is not feasible.

ACKNOWLEDGEMENTS

AuD acknowledges support by NASA through Chandra Award number TM1-22001B and GO2-23003X issued by the Chandra X-ray Observatory 27 Center, which is operated by the Smithsonian Astrophysical Observatory for and on behalf of NASA under contract NAS8-03060.

DATA AVAILABILITY STATEMENT

No new data was generated for this work. The software presented is available upon request from the authors.

REFERENCES

Babel J., Montmerle T., 1997, A&A, 323, 121
Berry I. D., Owocki S. P., Shultz M. E., ud Doula A., 2022, Monthly Notices of the Royal Astronomical Society, 511, 4815
Bolton C. T., Fullerton A. W., Bohlender D., Landstreet J. D., Gies D. R., 1987, in Slettebak A., Snow T. P., eds, IAU Colloq. 92: Physics of Be Stars. p. 82
Bolton C. T., Harmanec P., Lyons R. W., Odell A. P., Pyper D. M., 1998, A&A, 337, 183
Castor J. I., Abbott D. C., Klein R. I., 1975, ApJ, 195, 157
Das B., Chandra P., 2021, ApJ, 921, 9
David-Uraz A., et al., 2019, MNRAS, 487, 304
Eikenberry S. S., et al., 2014, ApJ, 784, L30
Erba C., Shultz M. E., Petit V., Fullerton A. W., Henrichs H. F., Kochukhov O., Rivinius T., Wade G. A., 2021, MNRAS, 506, 2296
Gayley K. G., 1995, ApJ, 454, 410
Grunhut J. H., et al., 2012a, MNRAS, 419, 1610
Grunhut J. H., et al., 2012b, Monthly Notices of the Royal Astronomical Society, 428, 1686
Grunhut J. H., et al., 2017, MNRAS, 465, 2432
Grunhut J. H., et al., 2022, MNRAS, 512, 1944
Havnes O., Goertz C. K., 1984, A&A, 138, 421
Hesser J. E., Ugarte P. P., Moreno H., 1977, ApJ, 216, L31
Høg E., et al., 2000, A&A, 355, L27

Howell S. B., et al., 2014, Publications of the Astronomical Society of the Pacific, 126, 398
Hubrig S., et al., 2015, Astronomy & Astrophysics, 578, L3
Hubrig S., Kholtygin A. F., Schöller M., Ilyin I., 2017, Monthly Notices of the Royal Astronomical Society: Letters, p. slx005
Jayaraman R., Hubrig S., Holdsworth D. L., Schöller M., Järvinen S., Kurtz D. W., Gagliano R., Ricker G. R., 2022, ApJ, 924, L10
Kochukhov O., Bagnulo S., 2006, A&A, 450, 763
Kochukhov O., Lundin A., Romanyuk I., Kudryavtsev D., 2011, ApJ, 726, 24
Kochukhov O., Shultz M., Neiner C., 2019, A&A, 621, A47
Krtička J., Janík J., Marková H., Mikulášek Z., Zverko J., Prvák M., Skarka M., 2013, A&A, 556, A18
Krtička J., Mikulášek Z., Zverko J., Žižňovský J., 2007, A&A, 470, 1089
Krtička J., Mikulášek Z., Henry G. W., Zverko J., Žižovský J., Skalický J., Zvěřina P., 2009, A&A, 499, 567
Krtička J., Mikulášek Z., Kurfürst P., Oksala M. E., 2022, A&A, 659, A37
Landstreet J. D., Borra E. F., 1978, ApJ, 224, L5
Leto P., et al., 2021, MNRAS, 507, 1979
Lightkurve Collaboration et al., 2018, Lightkurve: Kepler and TESS time series analysis in Python, Astrophysics Source Code Library (ascl:1812.013)
Mikulášek Z., et al., 2020, in Wade G., Alecian E., Bohlender D., Sigut A., eds, Proceedings of the Polish Astronomical Society Vol. 11, Stellar Magnetism: A Workshop in Honour of the Career and Contributions of John D. Landstreet. pp 46–53 (arXiv:1912.04121)
Munoz M. S., Wade G. A., Nazé Y., Puls J., Bagnulo S., Szymański M. K., 2020, MNRAS, 492, 1199
Oksala M. E., Wade G. A., Marcolino W. L. F., Grunhut J., Bohlender D., Manset N., Townsend R. H. D., 2010, Monthly Notices of the Royal Astronomical Society: Letters, 405, L51–L55
Oksala M. E., Wade G. A., Townsend R. H. D., Owocki S. P., Kochukhov O., Neiner C., Alecian E., Grunhut J., 2012, MNRAS, 419, 959
Oksala M. E., et al., 2015, MNRAS, 451, 2015
Owocki S. P., Cranmer S. R., 2018, MNRAS, 474, 3090
Owocki S. P., ud-Doula A., Sundqvist J. O., Petit V., Cohen D. H., Townsend R. H. D., 2016, MNRAS, 462, 3830
Owocki S. P., Shultz M. E., ud-Doula A., Sundqvist J. O., Townsend R. H. D., Cranmer S. R., 2020, MNRAS, 499, 5366
Owocki S. P., Shultz M. E., ud-Doula A., Chandra P., Das B., Leto P., 2022, MNRAS, 513, 1449
Petit V., et al., 2013, MNRAS, 429, 398
Petit V., et al., 2019, MNRAS, 489, 5669
Renson P., Catalano F. A., 2001, A&A, 378, 113
Ricker G. R., et al., 2015, Journal of Astronomical Telescopes, Instruments, and Systems, 1, 014003
Rivinius T., Štefl S., Townsend R. H. D., Baade D., 2008, Astronomy & Astrophysics, 482, 255–258
Rivinius T., Szeifert T., Barrera L., Townsend R. H. D., Štefl S., Baade D., 2010, Monthly Notices of the Royal Astronomical Society: Letters, 405, L46–L50
Rivinius T., Townsend R. H. D., Kochukhov O., Štefl S., Baade D., Barrera L., Szeifert T., 2013, MNRAS, 429, 177
Shultz M., Wade G. A., Rivinius T., Neiner C., Henrichs H., Marcolino W., MiMeS Collaboration 2017, MNRAS, 471, 2286
Shultz M., Rivinius T., Wade G. A., Alecian E., Petit V., 2018a, MNRAS, 475, 839
Shultz M., Kochukhov O., Wade G. A., Rivinius T., 2018b, MNRAS, 478, L39
Shultz M. E., et al., 2019a, MNRAS, 485, 1508
Shultz M. E., et al., 2019b, Monthly Notices of the Royal Astronomical Society, 490, 274
Shultz M. E., et al., 2020, MNRAS, 499, 5379
Shultz M. E., et al., 2021a, MNRAS, 504, 3203
Shultz M. E., Rivinius T., Wade G. A., Kochukhov O., Alecian E., David-Uraz A., Sikora J., 2021b, MNRAS, 504, 4850
Shultz M. E., et al., 2022, MNRAS, 513, 1429
Sikora J., et al., 2015, MNRAS, 451, 1928
Sikora J., Wade G. A., Power J., Neiner C., 2019a, MNRAS, 483, 2300
Sikora J., Wade G. A., Power J., Neiner C., 2019b, MNRAS, 483, 3127
Sikora J., et al., 2019c, MNRAS, 487, 4695
Townsend R. H. D., 2008, MNRAS, 389, 559
Townsend R. H. D., Owocki S. P., 2005, MNRAS, 357, 251
Townsend R. H. D., Owocki S. P., Groote D., 2005, ApJ, 630, L81
Townsend R. H. D., Oksala M. E., Cohen D. H., Owocki S. P., ud-Doula A., 2010, ApJ, 714, L318
Townsend R. H. D., et al., 2013, The Astrophysical Journal, 769, 33
Trigilio C., Leto P., Umana G., Leone F., Buemi C. S., 2004, A&A, 418, 593
Vink J. S., de Koter A., Lamers H. J. G. L. M., 2001, A&A, 369, 574
Wade G. A., et al., 2017, MNRAS, 465, 2517
Walker G., et al., 2003, PASP, 115, 1023
Wisniewski J. P., et al., 2015, The Astrophysical Journal, 811, L26
ud-Doula A., 2021, in MOBSTER-1 virtual conference: Stellar Variability as a Probe of Magnetic Fields in Massive Stars. p. 33, doi:10.5281/zenodo.5534944
ud-Doula A., Owocki S. P., 2002, ApJ, 576, 413
ud-Doula A., Townsend R. H. D., Owocki S. P., 2006, ApJ, 640, L191
ud-Doula A., Owocki S. P., Townsend R. H. D., 2008, MNRAS, 385, 97
ud-Doula A., Owocki S. P., Townsend R. H. D., 2009, MNRAS, 392, 1022